Coupling metastasis to pH sensing G Protein-coupled receptor-68 through first in class inhibitor identified in an in vivo chemical genetic screen

Charles H Williams*, Timothy Thayer, Quinn Wells, Mashhood Wani, Brittany Keyser, Charles C Hong*

Co-corresponding Authors: Charles.Williams@som.umaryland.edu, Charles.Hong@som.umaryland.edu

Abstract

Acidic milieu is a hallmark of glycolytic metabolism which occurs in cancerous cells. The effect of the acidic environment on cancer progression can be categorized into effects on tumor cell survival, tumor metastasis, inflammatory response, and blood vessels. Yet the underlying signaling and cell biological underpinnings of these phenomena are not well understood. Here, we describe, ogremorphen, a first in class inhibitor of proton-sensing GPCR GPR68. Discovered from a chemical genetic zebrafish screen, ogremorphen perturbed neural crest migration. Furthermore, ogremorphen was shown to inhibit migration in a number of human melanoma lines, which derive from the neural crest. Phenome-wide association study identified a natural variant that is aberrantly active and is associated with metastasis of common cancers. Our study suggests that GPR68 activity is associated with an increased ability for cancer cell migration and contributes to metastasis.

Introduction

Highly malignant, invasive, and metastatic cancers have markedly elevated glycolytic activity, producing an oncologically favorable acidotic extracellular environment; a phenomenon called the Warburg effect (Vander Heiden et al., 2009). This acidification (pHe < 7.4) of the environment is marked by increases in efflux

mechanisms H+ATPases and Na+-H+ exchangers (Martinez-Zaguilan et al., 1993; Martínez-Zaguilán et al., 1998; McLean et al., 2000; Sennoune et al., 2004). Furthermore, acidification promotes tumor malignancy, including metabolic reprogramming and invasiveness, the cellular mechanisms that mediate these phenomena are poorly understood (Justus et al., 2013; Webb et al., 2011). Investigations have shown that in numerous animal models of solid tumors, small molecule inhibition of NHE1 can have an effect on tumor growth and metastasis (Matthews et al., 2011). However, the cellular mechanisms triggered by the acidification of the tumor environment are still not wholly understood. In this investigation, identified as an inhibitor of proton-sensing GPCR (G protein-coupled receptor), GPR68, that modulates migratory behavior of melanoma cells in vitro and in vivo. Furthermore, Human Phenome-wide association study identified a functional variant in GPR68 that may increase the risk of tumor metastasis to bone and liver.

Results:

To discover novel small molecule modulators of embryonic development we conducted an unbiased screen of ~30,000 small molecules, assaying for their ability to induce phenotypic changes in morphology (Hao et al., 2013; Williams et al., 2015). We identified 5-ethyl-5'-naphthalen-1-ylspiro[1H-indole-3,2'-3H-1,3,4-thiadiazole]-2-one, here in called Ogremorphin (OGM), based on the phenotype of aberrant pigmentation (Figure 1 A, B,C). In addition to pigmentation defects, Ogremorphin reproducibly induced ventral curvature, wavy notochord, shortened body axis, craniofacial defects, and loss of retinal iridophores (Figure 3). The loss of melanophores, iridophores and craniofacial cartilage are consistent with abrogation of neural crest development (Kwak et al., 2013). Time course analysis showed that pigmentation was subject perturbation by OGM during a specific window of time correlated to neural crest migration(Figure 1D). To identify if neural crest progenitors were perturbed by OGM we stained for foxD3 and found no difference (Figure 1E). This suggests that the target of OGM plays a role affecting pigment cells after the formation of neural crest progenitors.

Since GPCRs represent >30% of targets for FDA approved small molecules and are known to modulate cell migration, we assessed for activity against 158 GPCRs based on its chemical structure; in a single point assay

and significantly inhibited LPA1, GPR14/UT2R, and GPR68/OGR1 (Figure 2A). Chemical segregation analysis of zebrafish phenotype was conducted to further identify the inhibitory activity responsible for the zebrafish phenotype. Commercially available inhibitors of LPAR1 (Ki16425) and GPR14 (SB657510) were both assayed and failed to induce a noticeable phenotype at concentrations up to 200X the IC50. Furthermore, a small scale structure-activity relationship around the core pharmacophore of OGM generated molecules that were similar to OGM but did not have LPAR1 activity (Figure 2B,C). The GPR68 inhibitory activity of OGM analogs segregated with the ability of the molecule to induce the phenotype in zebrafish. For further experiments OGM8345 resynthesized and used due to its submicromolar potency and GPR68 specificity (Supplemental 1-2). We considered the possibility of OGM8345 being an irreversible inhibitor so we incubated Chem1-OGR1 cells(Millipore) with 10uM OGM8345 for 4 hours, and after removing the compound stimulated with pH6.4 media. We found that the signal returned back towards baseline uninhibited levels in a rapid and time-dependent manner (Figure 2D). Taken together, the data suggest that OGM8345 is a reversible and highly specific inhibitor of GPR68.

Zebrafish GPR68 and human GPR68 have a high degree of homology, with 58.3% identity and 75.2% similarity(Supplemental 3A). Compared to this, in zebrafish, the proton-sensing GPCR family members GPR4 and GPR65 are 41.45% and 28.04% similar, respectively (Supplemental 3B). To determine if the loss of GPR68 activity causes neural crest defects in zebrafish we knocked down GPR68 using morpholino oligonucleotides. We found that the neural crest-specific phenotypes of iridophores, melanocyte, and craniofacial cartilage were all disrupted in a dose-dependent manner using 1.5 ng and 3 ng morpholino, the same amount of mismatch morpholino did not recapitulate the result (Fig 3). Additionally, the wavy notochord which is not known to be a neural crest-related phenotype was recapitulated in morphants as well. Taken together, the data suggest that the phenotypes seen in OGM treatment are due to loss of GPR68 activity and include causes defective neural crest development and wavy notochord formation.

Since there are numerous parallels are found between neural crest cells and cancer during migration, we examined whether OGM could inhibit the migration of cells in human melanoma cell lines (Oppitz et al., 2007;

Schriek et al., 2005; Sinnberg et al., 2018). In a scratch assay for migration of 3 human melanoma cell lines A2058, MeWo, and WM115, OGM8345 (5uM) treated cells migrated significantly less than the vehicle treated cells (Figure 4A, B). Previous studies with the MV3 melanoma cell line have shown that disruption of proton efflux with EIPA inhibition of NHE1 can also reduce melanoma motility (Ludwig et al., 2013; Schneider et al., 2009; Stock et al., 2007, 2005; Stüwe et al., 2007). We show that, although this effect is significant in A2058 and WM115, MeWo appears refractory to the inhibition(Figure 4 B). Although the expression of GPR68 and other proton-sensing receptors have been characterized in various skin cancers (Merkel cell carcinoma, dermatofibrosarcoma protuberans, atypical fibroxanthoma, and pleomorphic dermal sarcoma), expression in melanoma cell lines has not investigated (Nassios et al., 2019). All three of these melanoma cell lines express GPR68, but only WM115 cells did not express GPR4 or GPR65 (Supplemental 4). Furthermore, in a 3D model of melanoma extravasation, OGM treated WM115 cells migrated significantly less than the vehicle treated cells (Figure 4). Taken together this data suggests that GPR68 plays a critical role in melanoma migration in vitro.

Given the intriguing effects of OGM on melanoma cells *in vitro,* we sought corroborating clinical evidence by looking for variants in the *GPR68* gene in BioVU, a large DNA sequence database linked to electronic health records of Vanderbilt University Medical Center (Carroll et al., 2014; Denny et al., 2016, 2013). The database contained a very rare *GPR68* variant, rs61745752 (minor allele frequency of 0.00074 in TOPMED database), which encodes a c-terminal truncated version of GPR68 (E336X). Phenome-Wide Association Study (PheWAS) showed that this variant was associated with odds ratio of ~3 for secondary malignancy of bone, secondary malignant neoplasm of the liver, and ~4.9 for “acquired absence of breast,” indicative of breast cancer surgery (Figure 5A, B, Supplementary Table 1) (Carroll et al., 2014; Denny et al., 2013). The cases of bone and liver metastasis associated with the rs61745752 variant involved 10 individuals (Figure 5C). In 7 of the 10 variant carriers, bone or liver metastasis was noted at the time of initial cancer diagnosis or within 1 year of diagnosis. In total, of 70 rs61745752 variant carriers identified in BioVU, 11.4% (8) had diagnosis of malignant neoplasm of breast and 5.7% (4) had diagnosis of malignant breast cancer and metastasis to bone or liver, compared to 4.6% and 1.1% respectively, in noncarriers (Figure 5D). Taken together, the data suggests that rs61745752 could be a risk variant for metastatic potential of various cancer types.

Given the apparent association rs61745752 with cancer metastasis, we sought to determine functional consequence of the variant which causes a truncation after amino acid 335 (E336X). Mutations in the c-terminal tail of GPCRs can have a number of consequences including loss of desensitization, and inactivation (Li et al., 2012). GPCR desensitization is modulated through beta-arrestin binding to domains that are defined by GIRK phosphorylation (Ahn et al., 2003; Luttrell and Lefkowitz, 2002; Sente et al., 2018). Prediction of putative binding sites for beta-arrestin binding identified a putative beta-arrestin binding site in the c-terminal cytosolic tail of the receptor, downstream of the early termination site (Fig 6A) (Zhou et al., 2017). Transfection of GFP-tagged GPR68 (GPR68-GFP) and truncated GPR68 (336X-GFP) in HEK293T cells revealed that the truncation variant (335X-GFP) fails to internalize in response to stimulation, while the full-length (GPR68-GFP) internalizes in response to stimulation (Figure 6B,C). Loss of internalization can indicate loss of activity or loss of the ability to internalize through beta-arrestin. We assessed the activity of the truncation variant (336X-GFP) and found that the truncation variant still retained activity in SRE (serum response element) responsive luciferase assay, which is activated by GPCR stimulation, particularly those coupled with Gi and Gq, through activation of the MAPK pathway(Cheng et al., 2010) (Supplemental 6). Furthermore, the activity of the truncation variant was still inhibited by OGM (Fig 6D). Taken together the data suggests that rs61745752 is aberrantly active through the loss of desensitization.

Finally, given the increased odds ratio of breast cancer-related metastasis in rs61745752 carriers in BioVU, we investigated mutational burden and survival in the cBioPortal cohort (Cerami et al., 2012; Gao et al., 2013). We found that breast cancer patients harboring mutations in GPR68 had worse overall survival than those without (Supplemental 5). By contrast, the closely related members of the proton-sensing GPCR family GPR4 and GPR65 did not have similar effects on overall survival (Supplemental 5). To ascertain if GPR68 and its variant could modulate metastatic potential in breast cancer in vitro we utilized spheroid integrity and invasion assay (Gayan et al., 2017; Jung et al., 2019). Transient transfection in MCF7 cells of GFP, GPR68-GFP, 336X-GFP reveals that, 3 days post matrix addition the continuity of the outer ring of cells becomes disrupted by the inner core in GPR68-GFP and 336X-GFP transected spheroids (Figure 7A). The cells of the inner core

then extrude out into the matrix increasingly over 5-7 days post matrix addition (Figure 7A-C). Furthermore, the degree of invasion in the 336X-GFP spheroids was greater than that of GPR68-GFP (Figure 7B,C). Notably, the invasive cells from the inner core were primarily GFP+ (Figure 7D). Taken together, this data suggests that GPR68 and its variant rs61745752 are sufficient to induce a more invasive phenotype in noninvasive breast cancer MCF7 cells.

Discussion

Targeting proton dynamics, and the dysregulation of pH has emerged as a possible therapeutic avenue for cancer (Justus et al., 2013; Parks et al., 2013; Webb et al., 2011). GPR68 has been implicated in the regulation of cancer in diverse and sometimes divergent ways (Wiley et al., 2019). GPR68, when overexpressed in PC3 prostate cancer cells have significantly reduced metastasis (Singh et al., 2007). Furthermore, in ovarian cancer cells HEY1, overexpression of GPR68 reduced cell migration and increased cell adhesion (Ren and Zhang, 2011). However, in medulloblastoma, GPR68 activation increases TRPC4 activity which enhances tumor cell migration (Wei et al., 2017). Furthermore, GPR68 has been identified as a critical regulator of cancer-associated fibroblasts in colon cancer and pancreatic cancer (Horman et al., 2017; Riemann et al., 2015; Wiley et al., 2018; Zhu et al., 2016). These reports suggest that GPR68 plays a critical role in regulating cancer progression.

Our results demonstrate that Ogremorphin functions as a reversible GPR68 inhibitor, a first-in-class negative regulator of this pathway. Additionally, our studies uncover a novel role for GPR68 in zebrafish development. Previous studies have shown that GPR68 is expressed during the early development of zebrafish, and responds to acidification like its mammalian homolog (Mochimaru et al., 2015). We show that inhibition of GPR68 during neural crest migration affects the development of pigmentation and craniofacial cartilage formation. In Xenopus, v-atpase regulates pH in a regional manner to affect craniofacial morphogenesis (Adams et al., 2006; Vandenberg et al., 2011). Notably, recent studies of GPR68 have shown that the receptor senses flow and stretch (Wei et al., 2018; Xu et al., 2018). However, responses to both stimuli are dependent on mildly acidic conditions. While it is still not clear if GPR68 is sensing protons in neural crest cells or the surrounding tissues, this is the first data that suggests that there could be proton mediated signaling events

that are critical for normal embryonic development. Notably, treatment of zebrafish with some proton efflux machinery phenocopies OGM treatment while others do not (Supplemental 7). Further studies of potential proton gradient formation *in vivo* during development are ongoing.

Cellular effects of acidification have been studied in numerous cancers (Bhujwalla et al., 2001; Glunde et al., 2003; Hill et al., 2001; Justus et al., 2013; McLean et al., 2000; Miraglia et al., 2005; Nishisho et al., 2011; Parks et al., 2013; Rofstad et al., 2006; Stüwe et al., 2007; Webb et al., 2011). Recent studies have focused on the mechanisms through which the acidification and pH modulation affects cancer cell behavior through proton-sensing receptors such as GPR4, GPR65 and GPR68. (Castellone et al., 2011; Justus et al., 2013; Weiß et al., 2017; Wiley et al., 2018). It has been shown in both *in vitro* and *in vivo* models that acidification promotes melanoma cell migration (Ludwig et al., 2013; Martínez-Zaguilán et al., 1996; Peppicelli et al., 2014; Rofstad et al., 2006). Consistent with this observation, our studies with Ogremorphin suggests that melanoma cells sense acidification through GPR68 to modulate their migration. Furthermore, using a functional genomics approach, we show that a rare *GPR68* gene variant, which results in a C-terminal truncation removing the putative β-arrestin binding domain, causes a loss of receptor internalization and is associated with increased risk of metastasis in the BioVU cohort. Notably, these metastases were found in common cancers like colon, and breast and lung. In a separate cohort, cBioPortal shows that mutations in GPR68 associate with poor outcome in breast cancer. Finally, we show that GPR68-expressing cells drive instability of MCF7 spheroids when transiently expressed. Although mechanistic studies are ongoing, our data suggests that GPR68 can autonomously promote invasive behaviors in cancer and represents a potential pharmacological target for metastasis.

Figure Legends.

Fig 1. ***Discovery of Ogremorphin (OGM)***.**A** Structure of Ogremorphin, 5-ethyl-5' -naphthalen-1 -ylspiro[1H-indole -3,2'-3H-1,3,4-thiadiazole]-2-one. **B** Dorsal view of DMSO vehicle control treated zebrafish embryo at 48 hpf.**C** Dorsal view of OGM (10uM) treated zebrafish embryo at 48hpf. **D** Temporal phenotypic analysis; Embryos treated throughout development 0-36hpf had perturbed pigmentation. Embryos treated 6-36hpf had perturbed pigmentation. Embryos treated 12-36hpf had perturbed pigmentation. Embryos treated 18-36hpf had normal pigmentation Embryos treated with a short pulse 0-6hpf had normal pigmentation. **E Left,** Lateral view of zebrafish after in situ hybridization of FOXD3, **Right** Magnification of inset (Red Arrows: positive staining along dorsal ridge of the embryo).

Fig 2. ***OGM is a reversible inhibitor of GPR68.*** **A.** Results of Millipore GPCR screen, 158 GPCRs were tested for agonist and antagonist activity at 10uM. Only GPR68, LPA1 and GPR14 (UT2R) showed significant activity. **B** Core scaffold for OGM derivatives **C** Chemical Linkage analysis, Loss of LPA activity did not correlate with loss of phenotype in zebrafish. Commercial inhibitors of UT2R (SB657510, Sigma) and LPA1R (Ki16425, Sigma) did not recapitulate phenotype. **D** GPR68 activity is restored rapidly after washout of inhibitor. Time till 50% max ~52 minutes.

Fig 3. ***GPR68 Knockdown recapitulated OGM induced zebrafish phenotype*** Morpholino knockdown of GPR68 induces craniofacial dysmorphogenesis, loss of iridophores, disrupted pigmentation, and wavy notochord. Doses of 3ng induced more embryos with phenotype than 1.5ng. The 3ng dose of mismatch morpholino had little effect. These phenotypes are consistent with 10uM and 20uM OGM treatments.

Fig 4. ***OGM inhibits human melanoma migration*** **A.** WM115 cells used in scratch assay; OGM and EIPA both prevent wound closure compared to DMSO (CTL). **B** Quantification of inhibition of scratch assay across three melanoma lines. OGM inhibited migration in WM115, A2050 and MEWO cell lines. EIPA inhibited migration in WM115 and A2058 but not MeWo lines. **C** Schematic of agarose drop assay. WM115 cells were mixed into low melt agarose solution and single 10uL drops were seeded onto cell culture plates. After

solidifying, media containing OGM (5uM) or CTL (DMSO .05%) was added and wells were observed 5 days later **D** Immediately after media addition no cells are on the plate outside of the agarose gel in CTL or OGM. 5 days after seeding cells are observed outside of the gel (Black arrows) in CTL but not in OGM. Close observation of CTL reveals cells crossing out of the gel drop (Black Arrowheads). **E** Quantification on the number of cells that escaped from an average of 5 gel drop replicates.

Fig 5 **GPR68 variant Rs61745752 associated with oncological signals including metastasis** The variant RS61745752 was had 70 carriers in the BIOVU cohort. **A** Manhattan plot of Phenome-wide association study for the snp rs61745752 Phecodes vs odds ratio. **B** Table of breast cancer-related phenotypes such as an abnormal mammogram, an acquired absence of breast, mammary dysplasia, and metastasis to liver and bone. **C** Comparison of the number of breast cancer patients and the frequency of metastatic diagnosis between carriers and non-carriers in the BioVU cohort. **D** Individual carriers with cancer metastasis with ages at the time of cancer diagnosis and age a time of metastasis show that the metastasis signal is not exclusively due to breast cancer patients.

Fig 6 **Variant Rs61745752 is a functional c-terminal truncation A** Phosphocode prediction of beta-arrestin binding site downstream of amino acid 335. Sequence aligned with known beta-arrestin interaction domains of Rhodopsin and Vasopressin 2. **B** GPR68-GFP and 336X-GFP transfected HEK293 cells were stimulated with pH6.8 media for 5 minutes. GPR68-GFP had puncta (white arrows)in the cell, 336X-GFP did not form puncta under acidic conditions. **C** Quantification of the number of puncta in each cell n=20 **D** Representative results from Serum responsive element (SRE-) luciferase assay. SRE has low levels of activity in HEK293T cells. Compared to GFP controls, GPR68-GFP and 336X-GFP transfected cells had higher levels of activity. Incubation with OGM 10uM reduced the level of luciferase activity in both GPR68-GFP and 336X-GFP conditions (N=3 technical replicates)

Fig 7 **GPR68 activity destabilized MCF7 spheroids** MCF7 cells transfected with GFP, GPR68-GFP, and 336X-GFP were seeded in Ultra low attachment plates to form spheroids. And at 48 hours 1:4 geltrex matrix

was added. **A** GFP transfected spheroids have the typical structure of outer proliferative ring with an inner quiescent core GPR68-GFP and 336X-GFP expressing spheroids have an irregular structure with the outer proliferative ring no longer intact on day 3. On day 5 GPR68-GFP and 336X-GFP spheroids show outgrowths from where the outer ring is not intact. **B** Quantification of the number of spheroids without intact outer rings N=8 **C** Quantification of the size of the outgrowth from spheroids. **D** Visualization of GFP+ cells in spheroids reveal that GFP+ cells are the primary component of the spheroid outgrowths.

Supplemental Figure Legends.

Sup 1. ***HNMR of resynthesis of OGM8345***.

Sup 2. ***LCMS of resynthesis of OGM8345.***

Sup 3. ***Similarity and Identity between proton-sensing GPCRs*** **A** Identity and similarity between human and zebrafish orthologs. **B** Similarity of acid-sensing GPCRs in zebrafish.

Sup 4. ***RT PCR of proton-sensing GPCRs in human melanoma cell lines*****.**

Sup 5 **Mutations in GPR68 correlate with poor prognosis in Breast cancer** . **A** Kaplan-Mier plot generated in cBioportal of Breast cancer cohort carrying alterations in GPR68. (P=0.013) **B** Kaplan-Mier plot generated in cBioportal of Breast cancer cohort carrying alterations in GPR4 (P=0.785) **C** Kaplan-Mier plot generated in cBioportal of Breast cancer cohort carrying alterations in GPR65 (P=0.612)

Sup 6 **E336X-GFP plasmid is still active in SRE-luciferase assay** Composite of results from Serum responsive element (SRE-) luciferase assay. SRE has low levels of activity in HEK293T cells. Compared to GFP controls, GPR68-GFP and 336X-GFP transfected cells had higher levels of activity. (N=3 biological replicates done in triplicate)

Sup 7 **Proton efflux machinery inhibition phenocopies OGM treatment A** Table of proton efflux inhibitors used to treat embryos at 5hpf. Omeprazole and Lansoprazole both phenocopy OGM inhibition. **B** Representative images of DMSO control OGM treatment and omeprazole treated embryos.

Methods:

Chemical Screen

All zebrafish experiments were approved by Vanderbilt University Institutional Animal Care and Use Committee. Chemical screen for small molecules that perturb dorsoventral axis was performed as previously described (Chen et al., 2009; Hao et al., 2013; Williams et al., 2015; Yu et al., 2008)). Briefly, pairs of WT zebrafish were mated, and fertilized eggs were arrayed in 96-well microtiter plates (5 embryos/well) containing 100 l E3 water. At 4hpf, small molecule library from Vanderbilt High Throughput Screening Facility was added to each well to the final concentration of 10M. Embryos were incubated at 28.5C until 24 and 48hpf, when they were examined for gross morphologic changes indicative of dorsalization of the embryonic axis. A total of 30,000 compounds were screened.

Alcian Blue staining

Staged embryos and larvae were anesthetized with Tricaine and killed by immersion in 4% formaldehyde (prepared from paraformaldehyde, and buffered to pH 7 in phosphate-buffered saline (PBS)). The fixed animals were rinsed in acid–alcohol (0.37% HCl, 70% EtOH), and stained overnight in Alcian blue (Schilling et al.,1996a) After destaining in several changes of acid–alcohol, the preparations were rehydrated. Following rinsing and clearing in a solution of 50% glycerol and 0.25% KOH, the cartilages were visualized under a stereo microscope.

Whole-Mount Zebrafish In Situ Hybridization

In situ hybridization was performed as previously described (Westerfield, 2000). Zebrafish foxD3 probes were synthesized as previously described (Stewart et al., 2006)

Target Profiling Assays for GPCR

GPCR profiling assays were performed by Millipore (St. Louis, MO) using in cells expressing Gα15, a promiscuous G protein that enhances GPCR coupling to downstream Ca2+ signaling pathways.

Zebrafish Injections

OGR1 morpholino 5'-TTTTTCCAACCACATGTTCAGAGTC-3' and Mismatch morpholino 5'-CCTCTTACCTCAGTTACAATTTATA-3 was synthesized by Genetools. Morpholino and mRNA was injected as previously described (Westerfield, 2000)

RT-PCR

Melanoma cell lines were collected and RNA isolated with the RNeasy kit (Qiagen, Valencia, CA). After subsequent cDNA amplification using Superscript III (Invitrogen, Carlsbad, CA) samples were visualized in an agarose gel. Primer sequences found below:

Gene	Forward	Reverse
GPR4	CCCTCCTGTCATAATTCCATCC	TGGTCTACAGGGAAGAGATGAG
GPR65	TGGCTGTTGTCTACCCTTTG	CCACAACATGACAGCATTGAAG
GPR68	GTTTGAAGGCGGCAGAAATG	GTGGAATGAGGAGGCATGAA
GPR132	TTCAGGAGCATCAAGCAGAG	CGAAGCAGACTAGGAAGATGAC
GAPDH	GTTTGAAGGCGGCAGAAATG	GTGGAATGAGGAGGCATGAA

Cell Culture and Transfection

HEK293, HEK293T, MeWo, A2058 and MCF7 cells were cultured in DMEM supplemented with 10% FBS (GIBCO) and 1% penicillin-streptomycin (Cellgro). SW480 cells were cultured in RPMI supplemented with 10% FBS (GIBCO) and 1% penicillin-streptomycin (Cellgro). WM115 cells were cultured in DMEM/F12 supplemented with 10% FBS (GIBCO) and 1% penicillin-streptomycin (Cellgro).

Luciferase assay Transfection

12 well plates of cells were transfected with 1ug DNA using Lipofectamine 3000 with sre: luciferase and either GFP, GPR68-GFP or 336X-GFP. After 3 days these cells were then lysed, and cell extracts were subjected to Steady-Glo luciferase assay (Promega) according to the manufacturer's instructions. The results were normalized to cell titer, as determined using Cell Titer-Glo luminescence assay (Promega)

336X-GFP plasmid generation

A deletion between amino acid 336 and the beginning of GFP was generated from the MCSV:GPR68-GFP plasmid using the Q5 mutagenesis kit (NEB).

Agarose drop assay

WM115 cells were trypsinized and resuspended at 100,000 cells per mL in low melt agarose. A 10ul drop of the cell mixture was added to 12 well plate. After solidifying Normal culture media was added with either DMSO 0.5% or OGM 5uM. The area around the agarose drop was visualized manually with light microscopy. The cells were incubated for 5 days and visualized. Cells outside of the agarose drop were visualized and quantitated.

Scratch assay

Cells were grown to confluence and the cells were denuded with a P200 tip. Cells a media change was done to add fresh media, remove loose cells and add compounds OGM(5 uM) and EIPA (10 uM). The area of the scratch was observed 20 hours later.

PheWAS

We performed PheWAS was performed on snp variant rs61745752 using methods and code groupings previously described (Denny et al., 2016, 2013) using the R PheWAS package(Carroll et al., 2014), briefly, calculating comprehensive associations between SNPs and a total of 1645 clinical phenotypes derived from the International Classification of Disease, 9th CM (ICD-9) edition codes from the BioVU Cohort's EHR(electronic health record). The ICD-9 codes that are associated with each phenotype can be found at the PheWAS catalog located online at http://phewas.mc.vanderbilt.edu/. In brief, the PheWAS algorithm calculates case and control genotype distributions then calculates associated *P*-value using logistic regression, and allelic odds ratio (OR). For those cases in which observed counts fell below five, Fisher's exact test was used to calculate the *P*-value using the *R* statistical package. Cases for a given disease were defined as having at least two relevant ICD-9 codes on different days. The PheWAS code also defines relevant control groups for each disease or finding, such that patients with related diseases do not serve as controls for that disease (e.g., a patient with psoriatic arthritis cannot serve as a control for an analysis of rheumatoid arthritis)

Chem-1 OGR1/GPR68 recovery assay

Chem-1 OGR1/GPR68 cells from Millipore (St. Louis, MO) were plated in 96 well format and stained with Fluo-8. Using the Lionheart FX (Biotek) a baseline for 3 seconds was observed before Media was acidified using an automated injector to reach pH6.8. Cells were then dynamically monitored and change in fluorescence was quantified using Gen5 software (Biotek). Pretreatment of 10uM OGM8345 for 4 hours was used. Each well was only assayed once at the correct time interval after inhibitor removal.

Acknowledgments

FoxD3 in situ hybridization probes were a kind gift from Knapik lab (Vanderbilt University). A2058, MeWo, WM115 cells were a kind gift from Quaranta lab (Vanderbilt University). MSCV: OGR1-GFP herein called GPR68-GFP was a kind gift from Owen Witte (Howard Hughes Medical Institute). Thank you to the Vanderbilt

Institute for Clinical and Translational Research (VICTR) for de-identified electronic health record data and archived genetic data. This work was funded by NIGMS R01GM118557 (CCH) and 5UL1TR002243 (VICTR).

Bibliography

Adams, D.S., Robinson, K.R., Fukumoto, T., Yuan, S., Albertson, R.C., Yelick, P., Kuo, L., McSweeney, M., Levin, M., 2006. Early, H+-V-ATPase-dependent proton flux is necessary for consistent left-right patterning of non-mammalian vertebrates. Development 133, 1657–1671. doi:10.1242/dev.02341

Ahn, S., Nelson, C.D., Garrison, T.R., Miller, W.E., Lefkowitz, R.J., 2003. Desensitization, internalization, and signaling functions of beta-arrestins demonstrated by RNA interference. Proc Natl Acad Sci USA 100, 1740–1744. doi:10.1073/pnas.262789099

Bhujwalla, Z.M., Artemov, D., Aboagye, E., Ackerstaff, E., Gillies, R.J., Natarajan, K., Solaiyappan, M., 2001. The physiological environment in cancer vascularization, invasion and metastasis. Novartis Found. Symp. 240, 23–38; discussion 38.

Carroll, R.J., Bastarache, L., Denny, J.C., 2014. R PheWAS: data analysis and plotting tools for phenome-wide association studies in the R environment. Bioinformatics 30, 2375–2376. doi:10.1093/bioinformatics/btu197

Castellone, R.D., Leffler, N.R., Dong, L., Yang, L.V., 2011. Inhibition of tumor cell migration and metastasis by the proton-sensing GPR4 receptor. Cancer Lett. 312, 197–208. doi:10.1016/j.canlet.2011.08.013

Cerami, E., Gao, J., Dogrusoz, U., Gross, B.E., Sumer, S.O., Aksoy, B.A., Jacobsen, A., Byrne, C.J., Heuer, M.L., Larsson, E., Antipin, Y., Reva, B., Goldberg, A.P., Sander, C., Schultz, N., 2012. The cBio cancer genomics portal: an open platform for exploring multidimensional cancer genomics data. Cancer Discov. 2, 401–404. doi:10.1158/2159-8290.CD-12-0095

Chen, B., Dodge, M.E., Tang, W., Lu, J., Ma, Z., Fan, C.-W., Wei, S., Hao, W., Kilgore, J., Williams, N.S., Roth, M.G., Amatruda, J.F., Chen, C., Lum, L., 2009. Small molecule-mediated disruption of Wnt-dependent signaling in tissue regeneration and cancer. Nat. Chem. Biol. 5, 100–107. doi:10.1038/nchembio.137

Cheng, Z., Garvin, D., Paguio, A., Stecha, P., Wood, K., Fan, F., 2010. Luciferase Reporter Assay System for Deciphering GPCR Pathways. Curr. Chem. Genomics 4, 84–91. doi:10.2174/1875397301004010084

Denny, J.C., Bastarache, L., Ritchie, M.D., Carroll, R.J., Zink, R., Mosley, J.D., Field, J.R., Pulley, J.M., Ramirez, A.H., Bowton, E., Basford, M.A., Carrell, D.S., Peissig, P.L., Kho, A.N., Pacheco, J.A., Rasmussen, L.V., Crosslin, D.R., Crane, P.K., Pathak, J., Bielinski, S.J., Roden, D.M., 2013. Systematic comparison of phenome-wide association study of electronic medical record data and genome-wide association study data. Nat. Biotechnol. 31, 1102–1110. doi:10.1038/nbt.2749

Denny, J.C., Bastarache, L., Roden, D.M., 2016. Phenome-Wide Association Studies as a Tool to Advance Precision Medicine. Annu. Rev. Genomics Hum. Genet. 17, 353–373. doi:10.1146/annurev-genom-090314-024956

Gao, J., Aksoy, B.A., Dogrusoz, U., Dresdner, G., Gross, B., Sumer, S.O., Sun, Y., Jacobsen, A., Sinha, R., Larsson, E., Cerami, E., Sander, C., Schultz, N., 2013. Integrative analysis of complex cancer genomics and clinical profiles using the cBioPortal. Sci. Signal. 6, pl1. doi:10.1126/scisignal.2004088

Gayan, S., Teli, A., Dey, T., 2017. Inherent aggressive character of invasive and non-invasive cells dictates the in vitro migration pattern of multicellular spheroid. Sci. Rep. 7, 11527. doi:10.1038/s41598-017-10078-7

Glunde, K., Guggino, S.E., Solaiyappan, M., Pathak, A.P., Ichikawa, Y., Bhujwalla, Z.M., 2003. Extracellular acidification alters lysosomal trafficking in human breast cancer cells. Neoplasia 5, 533–545.

Hao, J., Ao, A., Zhou, L., Murphy, C.K., Frist, A.Y., Keel, J.J., Thorne, C.A., Kim, K., Lee, E., Hong, C.C., 2013. Selective small molecule targeting β-catenin function discovered by in vivo chemical genetic screen. Cell Rep. 4, 898–904. doi:10.1016/j.celrep.2013.07.047

Hill, R.P., De Jaeger, K., Jang, A., Cairns, R., 2001. pH, hypoxia and metastasis. Novartis Found. Symp. 240, 154–65; discussion 165.

Horman, S.R., To, J., Lamb, J., Zoll, J.H., Leonetti, N., Tu, B., Moran, R., Newlin, R., Walker, J.R., Orth, A.P., 2017. Functional profiling of microtumors to identify cancer associated fibroblast-derived drug targets.

Oncotarget 8, 99913–99930. doi:10.18632/oncotarget.21915
Jung, H.-Y., Fattet, L., Tsai, J.H., Kajimoto, T., Chang, Q., Newton, A.C., Yang, J., 2019. Apical-basal polarity inhibits epithelial-mesenchymal transition and tumour metastasis by PAR-complex-mediated SNAI1 degradation. Nat. Cell Biol. 21, 359–371. doi:10.1038/s41556-019-0291-8
Justus, C.R., Dong, L., Yang, L.V., 2013. Acidic tumor microenvironment and pH-sensing G protein-coupled receptors. Front. Physiol. 4, 354. doi:10.3389/fphys.2013.00354
Kwak, J., Park, O.K., Jung, Y.J., Hwang, B.J., Kwon, S.-H., Kee, Y., 2013. Live image profiling of neural crest lineages in zebrafish transgenic lines. Mol. Cells 35, 255–260. doi:10.1007/s10059-013-0001-5
Li, G., Zhou, Q., Yu, Y., Chen, L., Shi, Y., Luo, J., Benovic, J., Lu, J., Zhou, N., 2012. Identification and characterization of distinct C-terminal domains of the human hydroxycarboxylic acid receptor-2 that are essential for receptor export, constitutive activity, desensitization, and internalization. Mol. Pharmacol. 82, 1150–1161. doi:10.1124/mol.112.081307
Ludwig, F.T., Schwab, A., Stock, C., 2013. The Na+ /H+ -exchanger (NHE1) generates pH nanodomains at focal adhesions. J. Cell. Physiol. 228, 1351–1358. doi:10.1002/jcp.24293
Luttrell, L.M., Lefkowitz, R.J., 2002. The role of beta-arrestins in the termination and transduction of G-protein-coupled receptor signals. J. Cell Sci. 115, 455–465.
Martinez-Zaguilan, R., Lynch, R.M., Martinez, G.M., Gillies, R.J., 1993. Vacuolar-type H(+)-ATPases are functionally expressed in plasma membranes of human tumor cells. Am. J. Physiol. 265, C1015-29. doi:10.1152/ajpcell.1993.265.4.C1015
Martínez-Zaguilán, R., Martinez, G.M., Gomez, A., Hendrix, M.J., Gillies, R.J., 1998. Distinct regulation of pHin and [Ca2+]in in human melanoma cells with different metastatic potential. J. Cell. Physiol. 176, 196–205. doi:10.1002/(SICI)1097-4652(199807)176:1<196::AID-JCP21>3.0.CO;2-4
Martínez-Zaguilán, R., Seftor, E.A., Seftor, R.E., Chu, Y.W., Gillies, R.J., Hendrix, M.J., 1996. Acidic pH enhances the invasive behavior of human melanoma cells. Clin. Exp. Metastasis 14, 176–186.
Matthews, H., Ranson, M., Kelso, M.J., 2011. Anti-tumour/metastasis effects of the potassium-sparing diuretic amiloride: an orally active anti-cancer drug waiting for its call-of-duty? Int. J. Cancer 129, 2051–2061. doi:10.1002/ijc.26156
McLean, L.A., Roscoe, J., Jorgensen, N.K., Gorin, F.A., Cala, P.M., 2000. Malignant gliomas display altered pH regulation by NHE1 compared with nontransformed astrocytes. Am J Physiol, Cell Physiol 278, C676-88. doi:10.1152/ajpcell.2000.278.4.C676
Miraglia, E., Viarisio, D., Riganti, C., Costamagna, C., Ghigo, D., Bosia, A., 2005. Na+/H+ exchanger activity is increased in doxorubicin-resistant human colon cancer cells and its modulation modifies the sensitivity of the cells to doxorubicin. Int. J. Cancer 115, 924–929. doi:10.1002/ijc.20959
Mochimaru, Y., Azuma, M., Oshima, N., Ichijo, Y., Satou, K., Matsuda, K., Asaoka, Y., Nishina, H., Nakakura, T., Mogi, C., Sato, K., Okajima, F., Tomura, H., 2015. Extracellular acidification activates ovarian cancer G-protein-coupled receptor 1 and GPR4 homologs of zebra fish. Biochem. Biophys. Res. Commun. 457, 493–499. doi:10.1016/j.bbrc.2014.12.105
Nassios, A., Wallner, S., Haferkamp, S., Klingelhöffer, C., Brochhausen, C., Schreml, S., 2019. Expression of proton-sensing G-protein-coupled receptors in selected skin tumors. Exp. Dermatol. 28, 66–71. doi:10.1111/exd.13809
Nishisho, T., Hata, K., Nakanishi, M., Morita, Y., Sun-Wada, G.-H., Wada, Y., Yasui, N., Yoneda, T., 2011. The a3 isoform vacuolar type H^+-ATPase promotes distant metastasis in the mouse B16 melanoma cells. Mol. Cancer Res. 9, 845–855. doi:10.1158/1541-7786.MCR-10-0449
Oppitz, M., Busch, C., Schriek, G., Metzger, M., Just, L., Drews, U., 2007. Non-malignant migration of B16 mouse melanoma cells in the neural crest and invasive growth in the eye cup of the chick embryo. Melanoma Res. 17, 17–30. doi:10.1097/CMR.0b013e3280114f49
Parks, S.K., Chiche, J., Pouysségur, J., 2013. Disrupting proton dynamics and energy metabolism for cancer therapy. Nat. Rev. Cancer 13, 611–623. doi:10.1038/nrc3579

Peppicelli, S., Bianchini, F., Torre, E., Calorini, L., 2014. Contribution of acidic melanoma cells undergoing epithelial-to-mesenchymal transition to aggressiveness of non-acidic melanoma cells. Clin. Exp. Metastasis 31, 423–433. doi:10.1007/s10585-014-9637-6

Ren, J., Zhang, L., 2011. Effects of ovarian cancer G protein coupled receptor 1 on the proliferation, migration, and adhesion of human ovarian cancer cells. Chin. Med. J. 124, 1327–1332.

Riemann, A., Ihling, A., Thomas, J., Schneider, B., Thews, O., Gekle, M., 2015. Acidic environment activates inflammatory programs in fibroblasts via a cAMP-MAPK pathway. Biochim. Biophys. Acta 1853, 299–307. doi:10.1016/j.bbamcr.2014.11.022

Rofstad, E.K., Mathiesen, B., Kindem, K., Galappathi, K., 2006. Acidic extracellular pH promotes experimental metastasis of human melanoma cells in athymic nude mice. Cancer Res. 66, 6699–6707. doi:10.1158/0008-5472.CAN-06-0983

Schneider, L., Stock, C.-M., Dieterich, P., Jensen, B.H., Pedersen, L.B., Satir, P., Schwab, A., Christensen, S.T., Pedersen, S.F., 2009. The Na+/H+ exchanger NHE1 is required for directional migration stimulated via PDGFR-alpha in the primary cilium. J. Cell Biol. 185, 163–176. doi:10.1083/jcb.200806019

Schriek, G., Oppitz, M., Busch, C., Just, L., Drews, U., 2005. Human SK-Mel 28 melanoma cells resume neural crest cell migration after transplantation into the chick embryo. Melanoma Res. 15, 225–234.

Sennoune, S.R., Bakunts, K., Martínez, G.M., Chua-Tuan, J.L., Kebir, Y., Attaya, M.N., Martínez-Zaguilán, R., 2004. Vacuolar H+-ATPase in human breast cancer cells with distinct metastatic potential: distribution and functional activity. Am J Physiol, Cell Physiol 286, C1443-52. doi:10.1152/ajpcell.00407.2003

Sente, A., Peer, R., Srivastava, A., Baidya, M., Lesk, A.M., Balaji, S., Shukla, A.K., Babu, M.M., Flock, T., 2018. Molecular mechanism of modulating arrestin conformation by GPCR phosphorylation. Nat. Struct. Mol. Biol. 25, 538–545. doi:10.1038/s41594-018-0071-3

Singh, L.S., Berk, M., Oates, R., Zhao, Z., Tan, H., Jiang, Y., Zhou, A., Kirmani, K., Steinmetz, R., Lindner, D., Xu, Y., 2007. Ovarian cancer G protein-coupled receptor 1, a new metastasis suppressor gene in prostate cancer. J Natl Cancer Inst 99, 1313–1327. doi:10.1093/jnci/djm107

Sinnberg, T., Levesque, M.P., Krochmann, J., Cheng, P.F., Ikenberg, K., Meraz-Torres, F., Niessner, H., Garbe, C., Busch, C., 2018. Wnt-signaling enhances neural crest migration of melanoma cells and induces an invasive phenotype. Mol. Cancer 17, 59. doi:10.1186/s12943-018-0773-5

Stewart, R.A., Arduini, B.L., Berghmans, S., George, R.E., Kanki, J.P., Henion, P.D., Look, A.T., 2006. Zebrafish foxd3 is selectively required for neural crest specification, migration and survival. Dev. Biol. 292, 174–188. doi:10.1016/j.ydbio.2005.12.035

Stock, C., Gassner, B., Hauck, C.R., Arnold, H., Mally, S., Eble, J.A., Dieterich, P., Schwab, A., 2005. Migration of human melanoma cells depends on extracellular pH and Na+/H+ exchange. J Physiol (Lond) 567, 225–238. doi:10.1113/jphysiol.2005.088344

Stock, C., Mueller, M., Kraehling, H., Mally, S., Noël, J., Eder, C., Schwab, A., 2007. pH nanoenvironment at the surface of single melanoma cells. Cell. Physiol. Biochem. 20, 679–686. doi:10.1159/000107550

Stüwe, L., Müller, M., Fabian, A., Waning, J., Mally, S., Noël, J., Schwab, A., Stock, C., 2007. pH dependence of melanoma cell migration: protons extruded by NHE1 dominate protons of the bulk solution. J Physiol (Lond) 585, 351–360. doi:10.1113/jphysiol.2007.145185

Vandenberg, L.N., Morrie, R.D., Adams, D.S., 2011. V-ATPase-dependent ectodermal voltage and pH regionalization are required for craniofacial morphogenesis. Dev. Dyn. 240, 1889–1904. doi:10.1002/dvdy.22685

Vander Heiden, M.G., Cantley, L.C., Thompson, C.B., 2009. Understanding the Warburg effect: the metabolic requirements of cell proliferation. Science 324, 1029–1033. doi:10.1126/science.1160809

Webb, B.A., Chimenti, M., Jacobson, M.P., Barber, D.L., 2011. Dysregulated pH: a perfect storm for cancer progression. Nat. Rev. Cancer 11, 671–677. doi:10.1038/nrc3110

Wei, W.-C., Bianchi, F., Wang, Y.-K., Tang, M.-J., Ye, H., Glitsch, M.D., 2018. Coincidence Detection of Membrane Stretch and Extracellular pH by the Proton-Sensing Receptor OGR1 (GPR68). Curr. Biol. 28,

3815–3823.e4. doi:10.1016/j.cub.2018.10.046
Wei, W.-C., Huang, W.-C., Lin, Y.-P., Becker, E.B.E., Ansorge, O., Flockerzi, V., Conti, D., Cenacchi, G., Glitsch, M.D., 2017. Functional expression of calcium-permeable canonical transient receptor potential 4-containing channels promotes migration of medulloblastoma cells. J Physiol (Lond) 595, 5525–5544. doi:10.1113/JP274659
Weiß, K.T., Fante, M., Köhl, G., Schreml, J., Haubner, F., Kreutz, M., Haverkampf, S., Berneburg, M., Schreml, S., 2017. Proton-sensing G protein-coupled receptors as regulators of cell proliferation and migration during tumor growth and wound healing. Exp. Dermatol. 26, 127–132. doi:10.1111/exd.13209
Westerfield, M., 2000. The zebrafish book : a guide for the laboratory use of zebrafish, 4th ed. University of Oregon Press, Eugene, OR.
Wiley, S.Z., Sriram, K., Liang, W., Chang, S.E., French, R., McCann, T., Sicklick, J., Nishihara, H., Lowy, A.M., Insel, P.A., 2018. GPR68, a proton-sensing GPCR, mediates interaction of cancer-associated fibroblasts and cancer cells. FASEB J. 32, 1170–1183. doi:10.1096/fj.201700834R
Wiley, S.Z., Sriram, K., Salmerón, C., Insel, P.A., 2019. GPR68: an emerging drug target in cancer. Int. J. Mol. Sci. 20. doi:10.3390/ijms20030559
Williams, C.H., Hempel, J.E., Hao, J., Frist, A.Y., Williams, M.M., Fleming, J.T., Sulikowski, G.A., Cooper, M.K., Chiang, C., Hong, C.C., 2015. An in vivo chemical genetic screen identifies phosphodiesterase 4 as a pharmacological target for hedgehog signaling inhibition. Cell Rep. 11, 43–50. doi:10.1016/j.celrep.2015.03.001
Xu, J., Mathur, J., Vessières, E., Hammack, S., Nonomura, K., Favre, J., Grimaud, L., Petrus, M., Francisco, A., Li, J., Lee, V., Xiang, F.-L., Mainquist, J.K., Cahalan, S.M., Orth, A.P., Walker, J.R., Ma, S., Lukacs, V., Bordone, L., Bandell, M., Patapoutian, A., 2018. GPR68 senses flow and is essential for vascular physiology. Cell 173, 762–775.e16. doi:10.1016/j.cell.2018.03.076
Yu, P.B., Hong, C.C., Sachidanandan, C., Babitt, J.L., Deng, D.Y., Hoyng, S.A., Lin, H.Y., Bloch, K.D., Peterson, R.T., 2008. Dorsomorphin inhibits BMP signals required for embryogenesis and iron metabolism. Nat. Chem. Biol. 4, 33–41. doi:10.1038/nchembio.2007.54
Zhou, X.E., He, Y., de Waal, P.W., Gao, X., Kang, Y., Van Eps, N., Yin, Y., Pal, K., Goswami, D., White, T.A., Barty, A., Latorraca, N.R., Chapman, H.N., Hubbell, W.L., Dror, R.O., Stevens, R.C., Cherezov, V., Gurevich, V.V., Griffin, P.R., Ernst, O.P., Xu, H.E., 2017. Identification of Phosphorylation Codes for Arrestin Recruitment by G Protein-Coupled Receptors. Cell 170, 457–469.e13. doi:10.1016/j.cell.2017.07.002
Zhu, H., Guo, S., Zhang, Y., Yin, J., Yin, W., Tao, S., Wang, Y., Zhang, C., 2016. Proton-sensing GPCR-YAP Signalling Promotes Cancer-associated Fibroblast Activation of Mesenchymal Stem Cells. Int. J. Biol. Sci. 12, 389–396. doi:10.7150/ijbs.13688

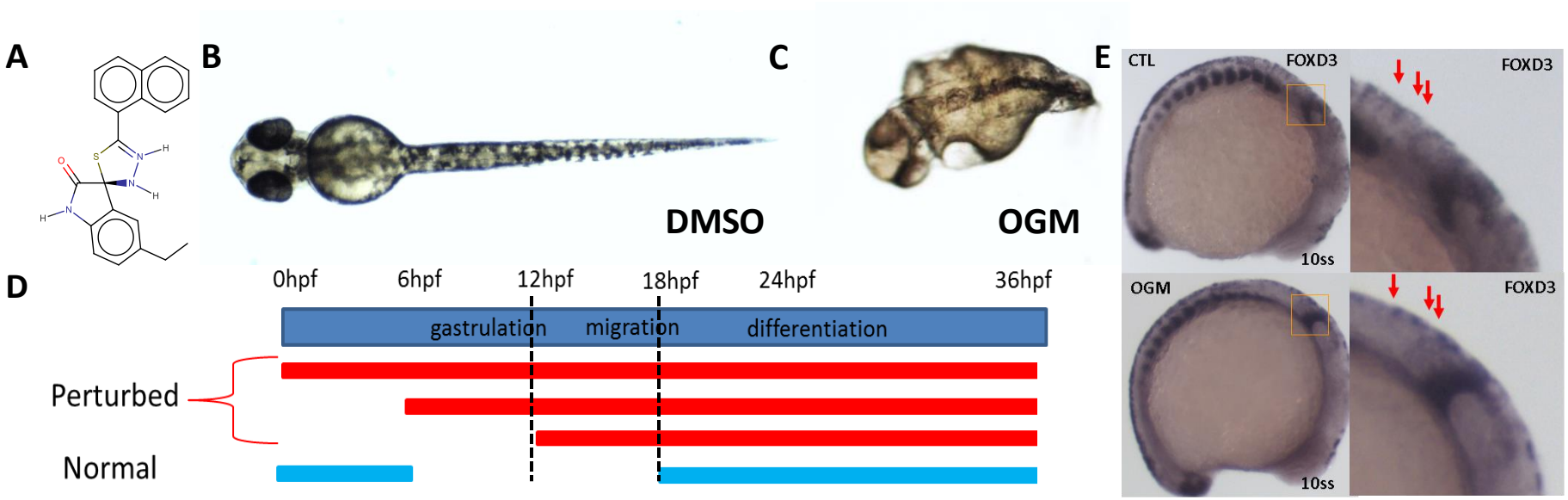
A
B
C
E
DMSO
OGM
D
0hpf
6hpf
12hpf
18hpf
24hpf
36hpf
gastrulation
migration
differentiation
Perturbed
Normal
CTL
FOXD3
FOXD3
10ss
OGM
FOXD3
10ss

Fig 1

A

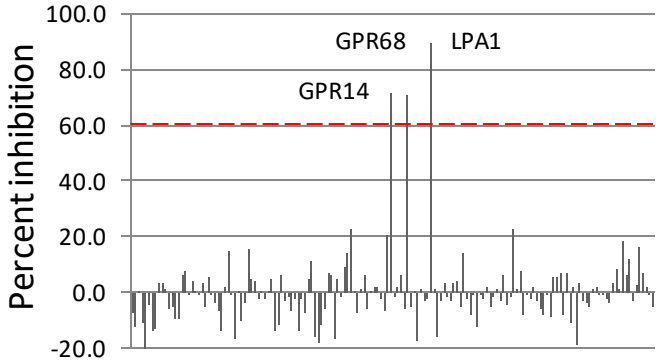

B

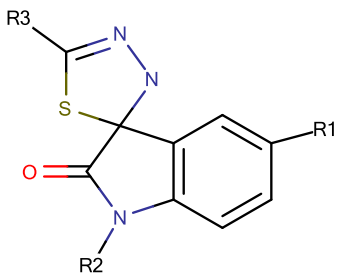

C

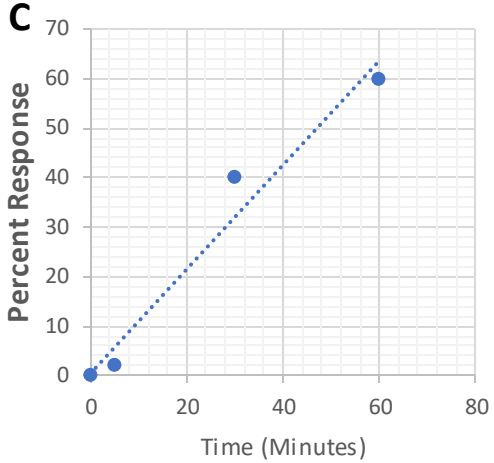

D

ID	R1	R2	R3	Phenotype	GPR68[μM]	LPA1[μM]
1294	H	Methyl	Benz	**Y**	0.81	----
8437	Methyl	H	Benz	**Y**	0.76	6.4
8345	Ethyl	H	Benz	**Y**	0.71	----
2440	Ethyl	H	2-Phen	**Y**	3.4	1.7
4906	H	Methyl	Napth	**Y**	1.5	----
OGM	Ethyl	H	Napth	**Y**	0.16	8.7
LPAi	-	-	-	N	-	0.25
UT2i	-	-	-	N	-	-

Fig 2

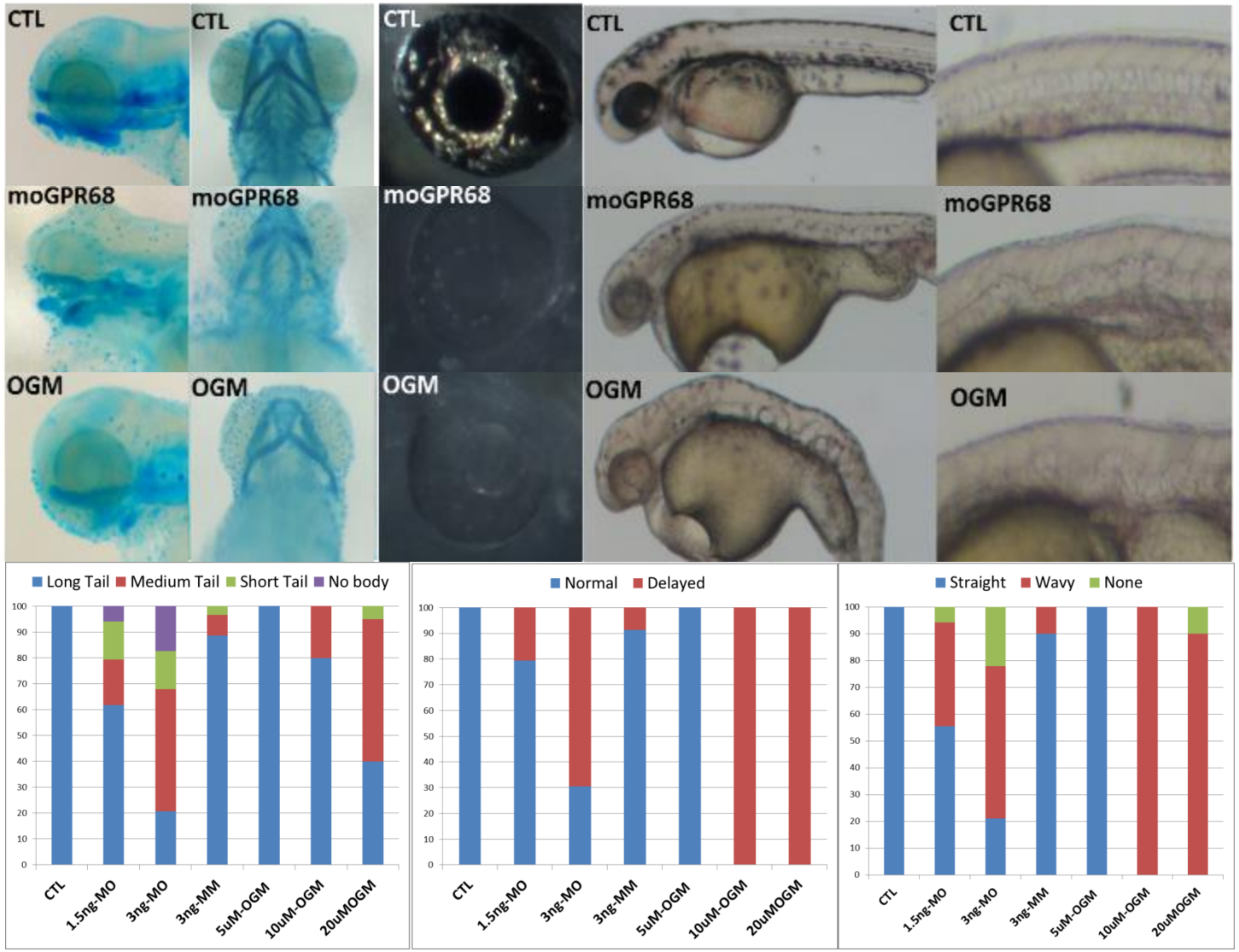
CTL
CTL
CTL
CTL
CTL
moGPR68
moGPR68
moGPR68
moGPR68
moGPR68
OGM
OGM
OGM
OGM
OGM
Long Tail
Medium Tail
Short Tail
No body
Normal
Delayed
Straight
Wavy
None
100
90
80
70
60
50
40
30
20
10
0
CTL
1.5ng-MO
3ng-MO
3ng-MM
5uM-OGM
10uM-OGM
20uMOGM

Fig 3

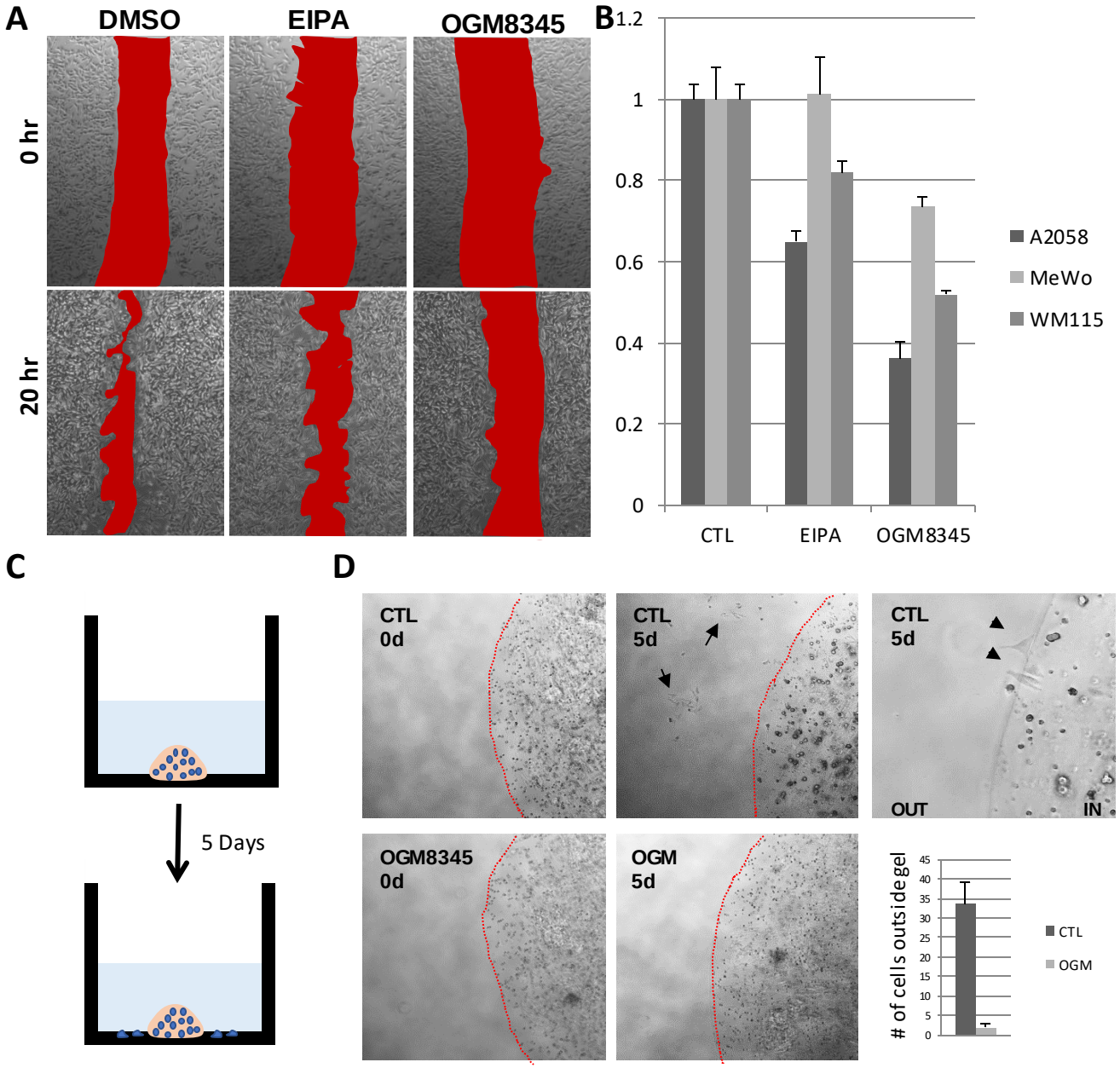
A
DMSO
EIPA
OGM8345
0 hr
20 hr
B
1.2
1
0.8
0.6
0.4
0.2
0
CTL
EIPA
OGM8345
A2058
MeWo
WM115
C
5 Days
D
CTL 0d
CTL 5d
CTL 5d
OUT
IN
OGM8345 0d
OGM 5d
# of cells outside gel
45
40
35
30
25
20
15
10
5
0
CTL
OGM

Fig 4

A

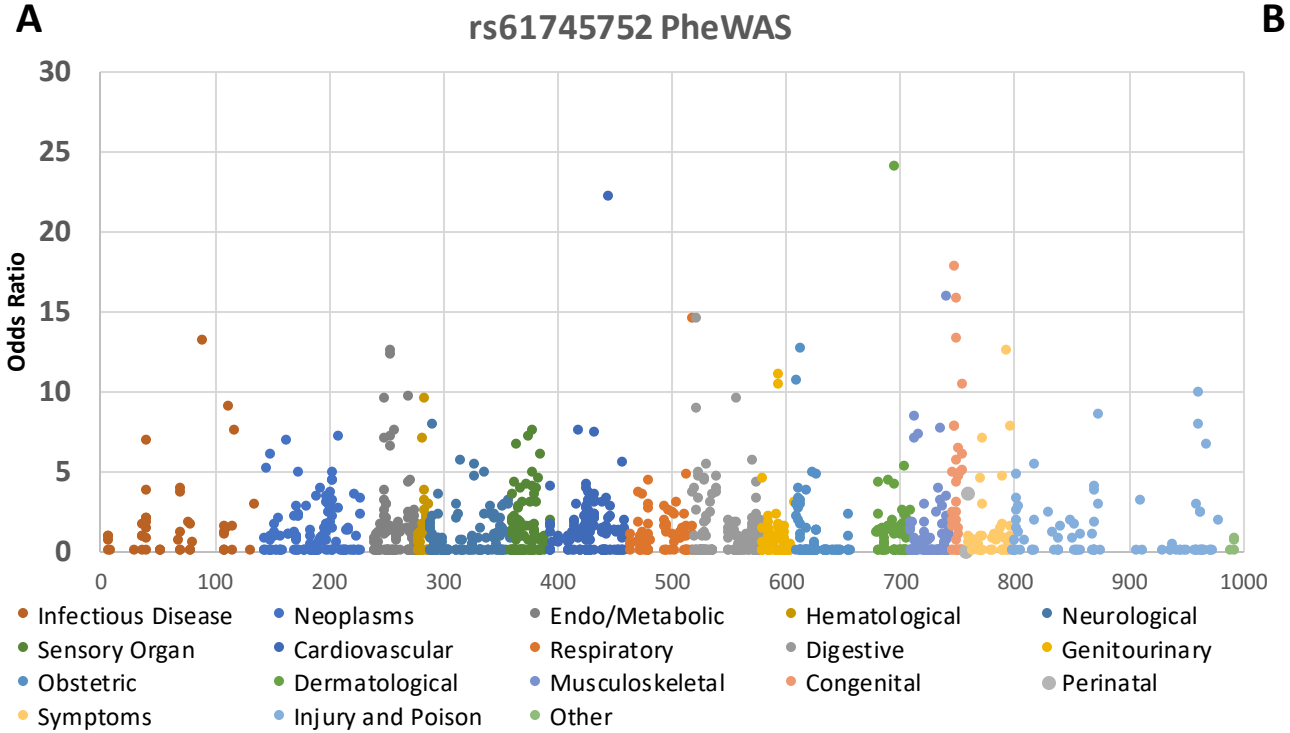

B

phewas_description	OR	P	Carriers w Dis.	Carriers Unaffected
Secondary malignant neoplasm of liver	3.3	0.00385	7	45
Secondary malignancy of bone	3.0	0.01277	6	45
Abnormal Mammogram	2.6	0.02372	8	54
Acquired absence of breast	4.9	0.00389	4	53

C

Case	Primary Cancer	Age, First Cancer Dx	Age, Bone Met (ICD9 198.5)	Age, Liver Met (ICD9 197.7)
1	Breast	44	44	49
2	Breast	56	60	60
3	Breast	68	NA	72
4	Breast	73	87	NA
5	Colon	62	NA	62
6	Colon	72	NA	72
7	Colon	79	79	NA
8	Lung	67	67	NA
9	Adrenal	44	45	45
10	Prostate	62	76	NA

D

	Carriers	Non-carriers	P-value
Total	70	31579	
Malignant neoplasm of breast	8 (11.4%)	1437 (4.6%)	0.0136
Malignant breast cancer and metastasis to bone or liver	4 (5.7%)	362 (1.1%)	0.0026

Fig 5

A

PREDICTED ARRESTIN BINDING DOMAIN

Rhodopsin	329	G	D	D	E	A	S	A	pT	V	-	pS	K	T	E	T	S	Q	V
Vasopressin 2	350	S	L	G	P	Q	D	E	pS	C	pT	pT	A	S	pS	S	L	A	K
GPR68	331	P	L	G	A	P	E	A	pS	G	K	pS	G	A	Q	G	E	E	E
rs61745752	331	P	L	G	A	P	X												

B

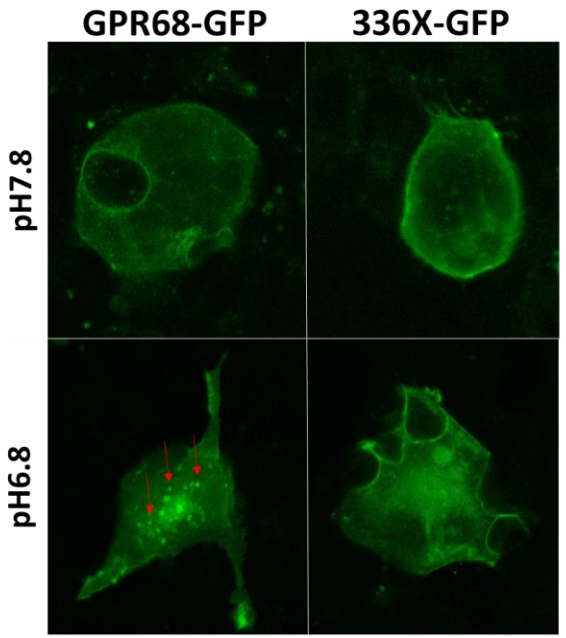

C

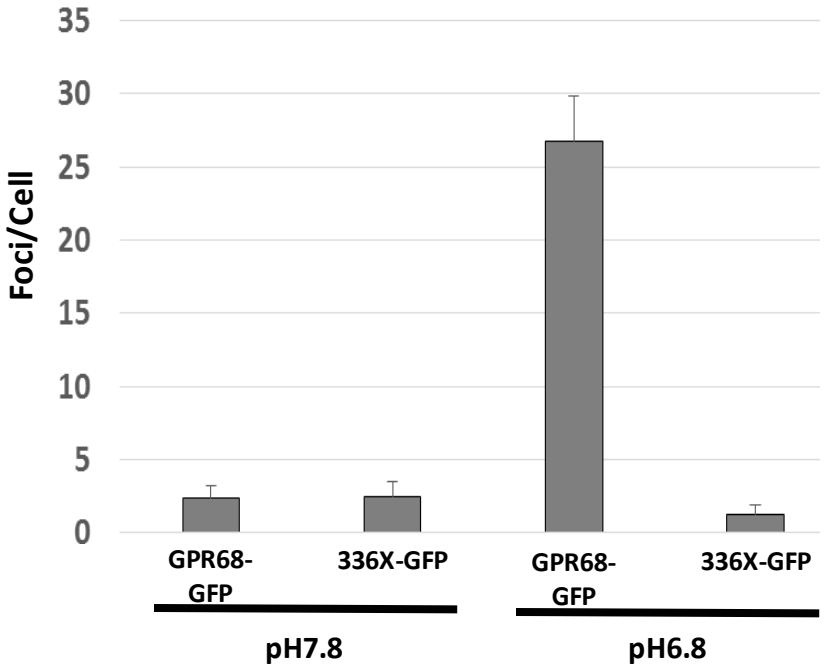

D

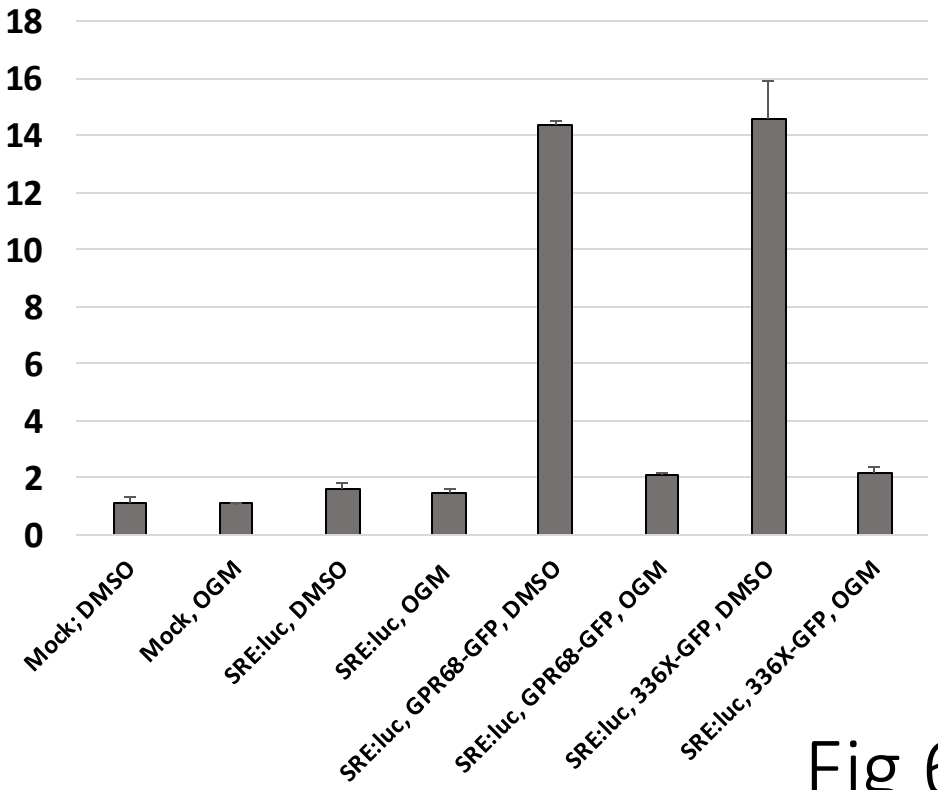

Fig 6

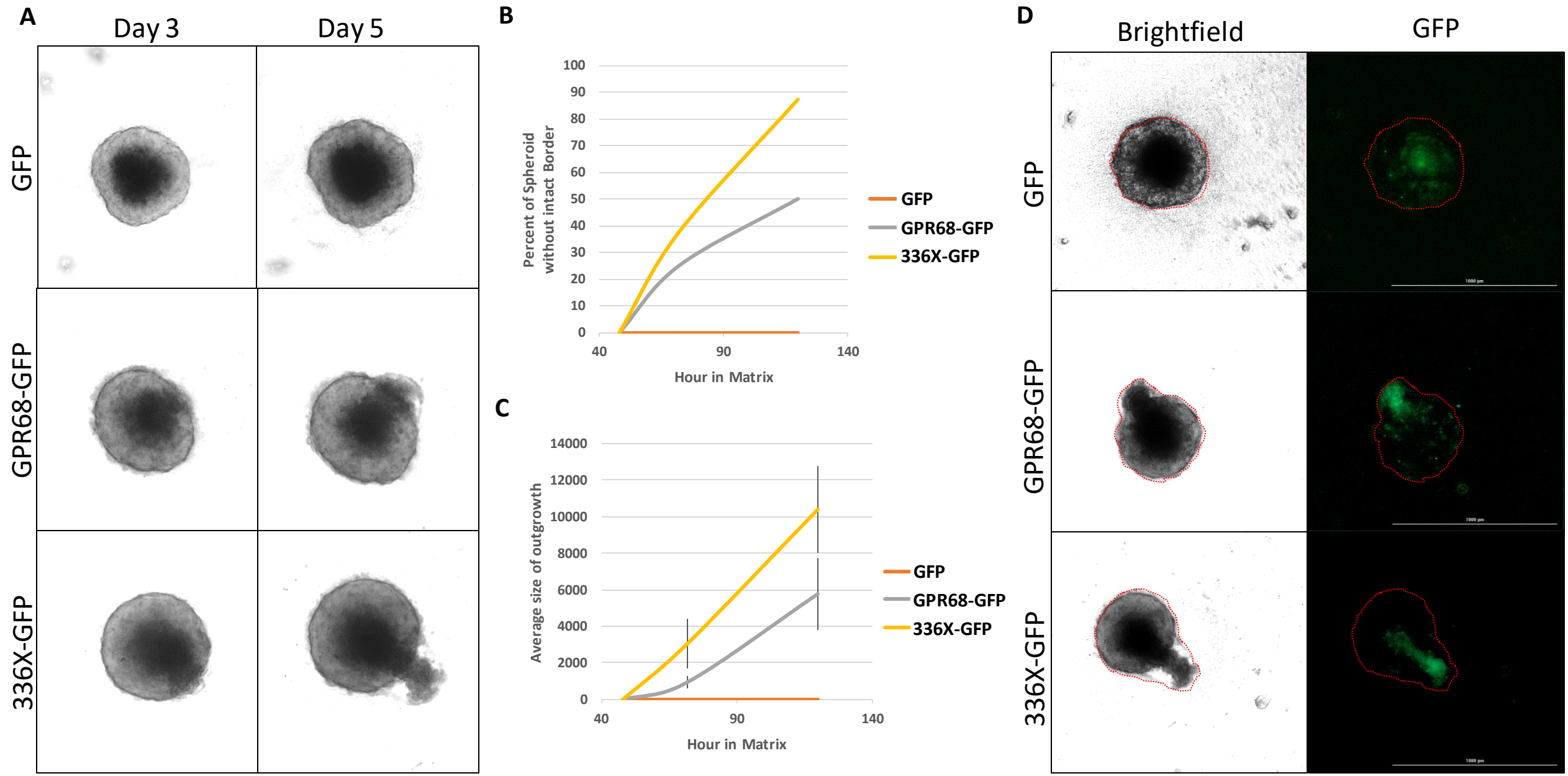
A
Day 3
Day 5
GFP
GPR68-GFP
336X-GFP
B
Percent of Spheroid without intact Border
100
90
80
70
60
50
40
30
20
10
0
40
90
140
Hour in Matrix
GFP
GPR68-GFP
336X-GFP
C
Average size of outgrowth
14000
12000
10000
8000
6000
4000
2000
0
40
90
140
Hour in Matrix
GFP
GPR68-GFP
336X-GFP
D
Brightfield
GFP
GFP
GPR68-GFP
336X-GFP

Fig 7

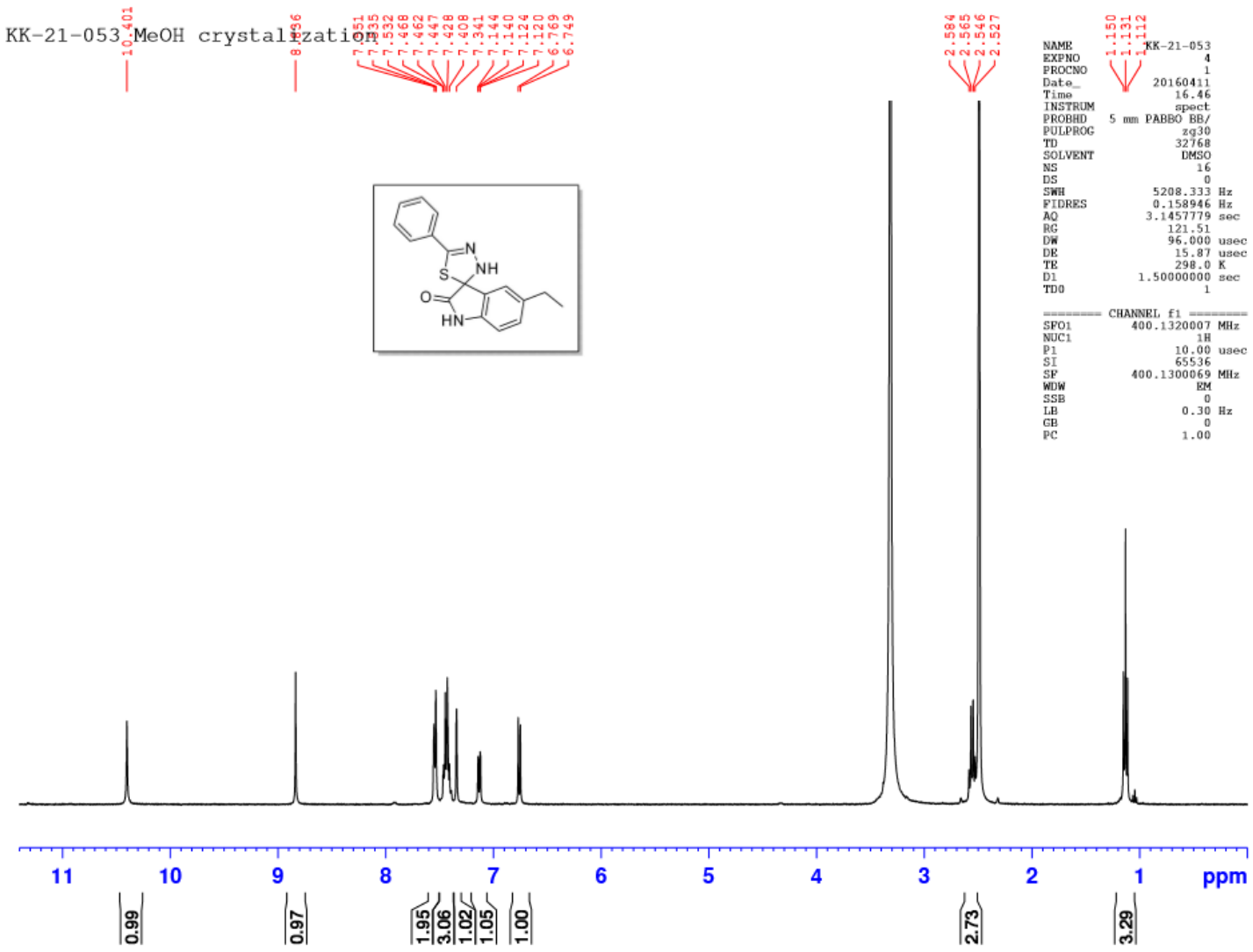
KK-21-053 MeOH crystallization
10.401
8.936
7.551
7.535
7.532
7.468
7.462
7.447
7.428
7.408
7.341
7.144
7.140
7.124
7.120
6.769
6.749
2.584
2.565
2.546
2.527
1.150
1.131
1.112
NAME KK-21-053
EXPNO 4
PROCNO 1
Date_ 20160411
Time 16.46
INSTRUM spect
PROBHD 5 mm PABBO BB/
PULPROG zg30
TD 32768
SOLVENT DMSO
NS 16
DS 0
SWH 5208.333 Hz
FIDRES 0.158946 Hz
AQ 3.1457779 sec
RG 121.51
DW 96.000 usec
DE 15.87 usec
TE 298.0 K
D1 1.50000000 sec
TD0 1
======== CHANNEL f1 ========
SFO1 400.1320007 MHz
NUC1 1H
P1 10.00 usec
SI 65536
SF 400.1300069 MHz
WDW EM
SSB 0
LB 0.30 Hz
GB 0
PC 1.00
N
NH
S
O
HN
11
10
9
8
7
6
5
4
3
2
1
ppm
0.99
0.97
1.95
3.06
1.02
1.05
1.00
2.73
3.29

Sup 1

Peak #	Time	Area % UV215	Area % UV254	Area % TIC(+)	BPM	Area Abs UV215	Area Abs UV254	Area Abs TIC(+)
1	0.241	37.6	0.0	5.2	157.2	658.96	0	81116.66
2	0.349	0.0	0.0	9.3	159.2	0	0	144753.36
3	1.200	62.4	100.0	85.5	310.1	1093.91	580.14	1333471.38

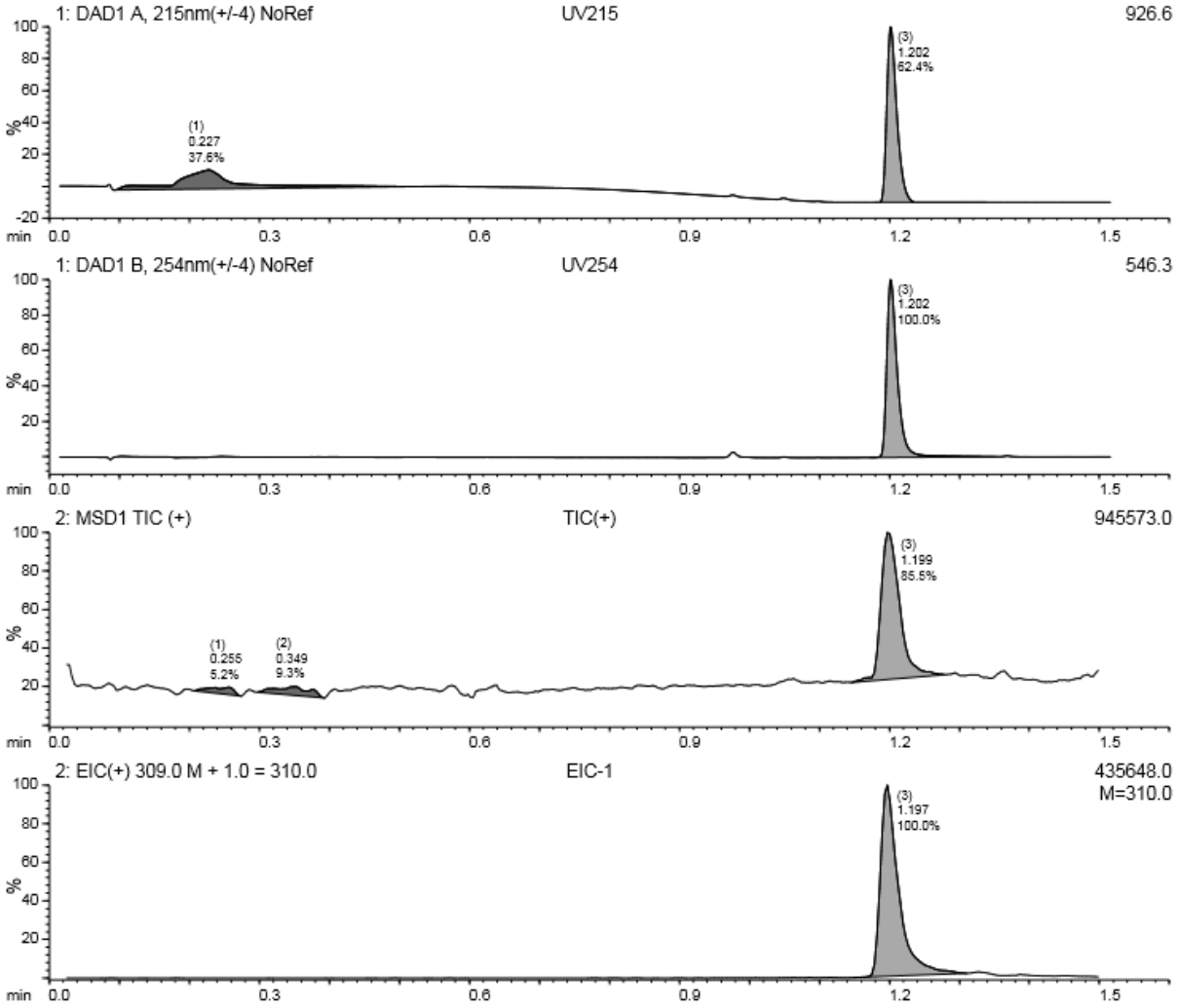

Sup 2

A

	Identity % (AA)	Similarity % (AA)
Hs. GPR65 vs zfGPR65	39	58.8
Hs. GPR68 vs zfGPR68	58.3	75.2
Hs. GPR4 vs zfGPR4	74.1	85.2

B

	zfGPR65	zfGPR68	zfGPR4
zfGPR65	100	28.04	30.61
zfGPR68	28.04	100	41.45
zfGPR4	30.61	41.45	100

Sup 3

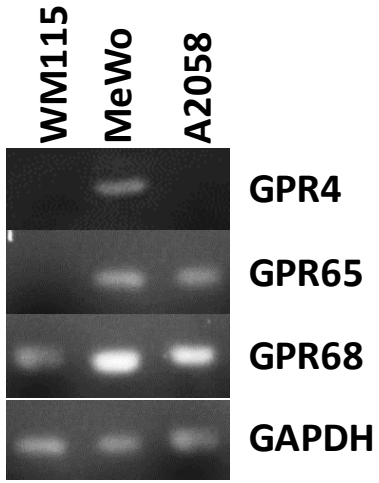

Sup 4

A

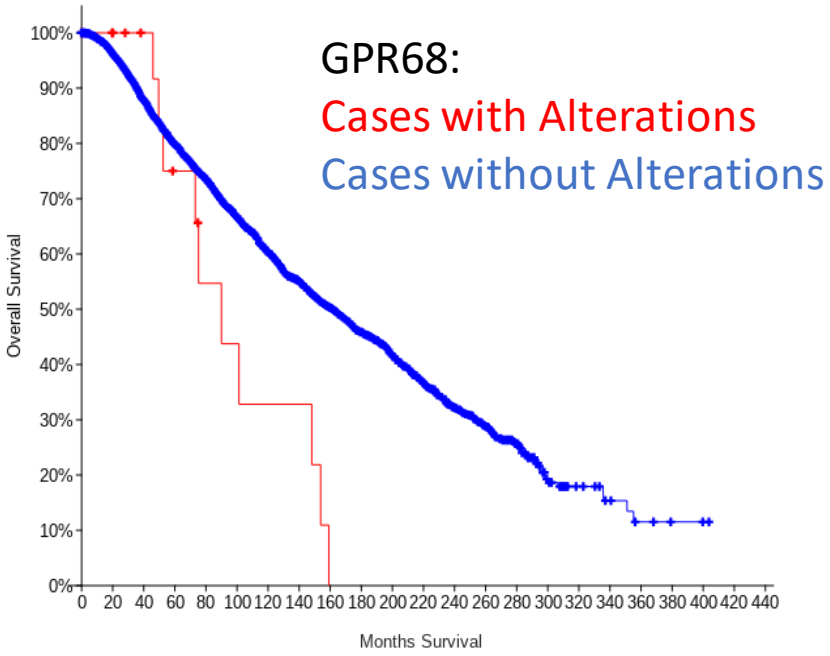

	Number of Cases, Total	Number of Cases, Deceased	Median Months Survival
Cases with Alterations in GPR68	18	10	89.96
Cases without Alterations in GPR68	6447	1879	161.7

B

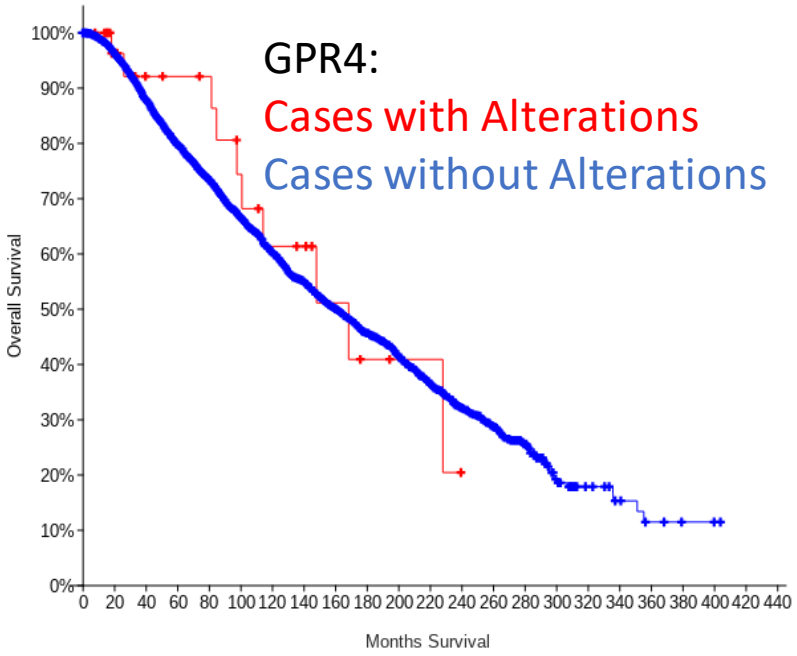

	Number of Cases, Total	Number of Cases, Deceased	Median Months Survival
Cases with Alterations in GPR4	32	10	168.2
Cases without Alterations in GPR4	6433	1879	160.3

C

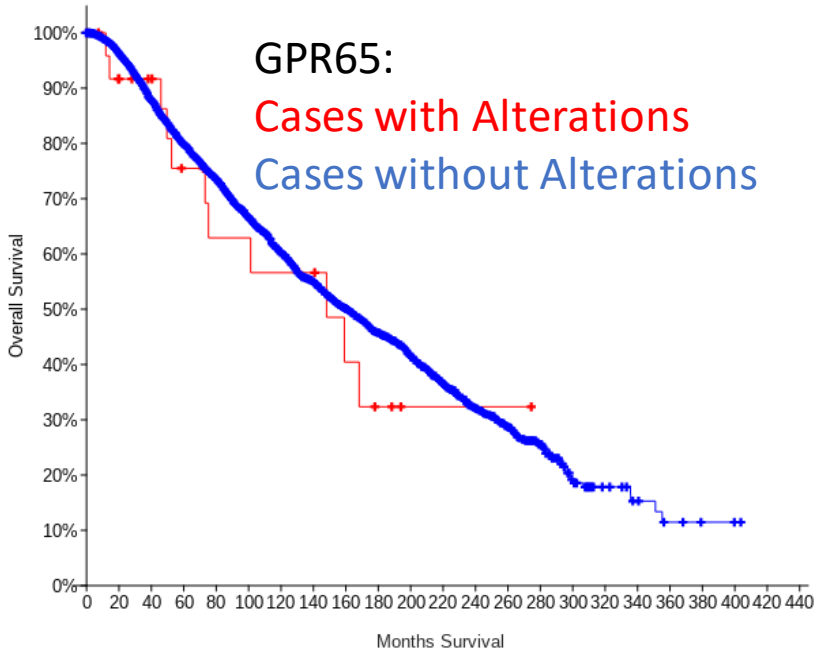

	Number of Cases, Total	Number of Cases, Deceased	Median Months Survival
Cases with Alterations in GPR65	27	11	148.1
Cases without Alterations in GPR65	6438	1878	160.4

Sup 5

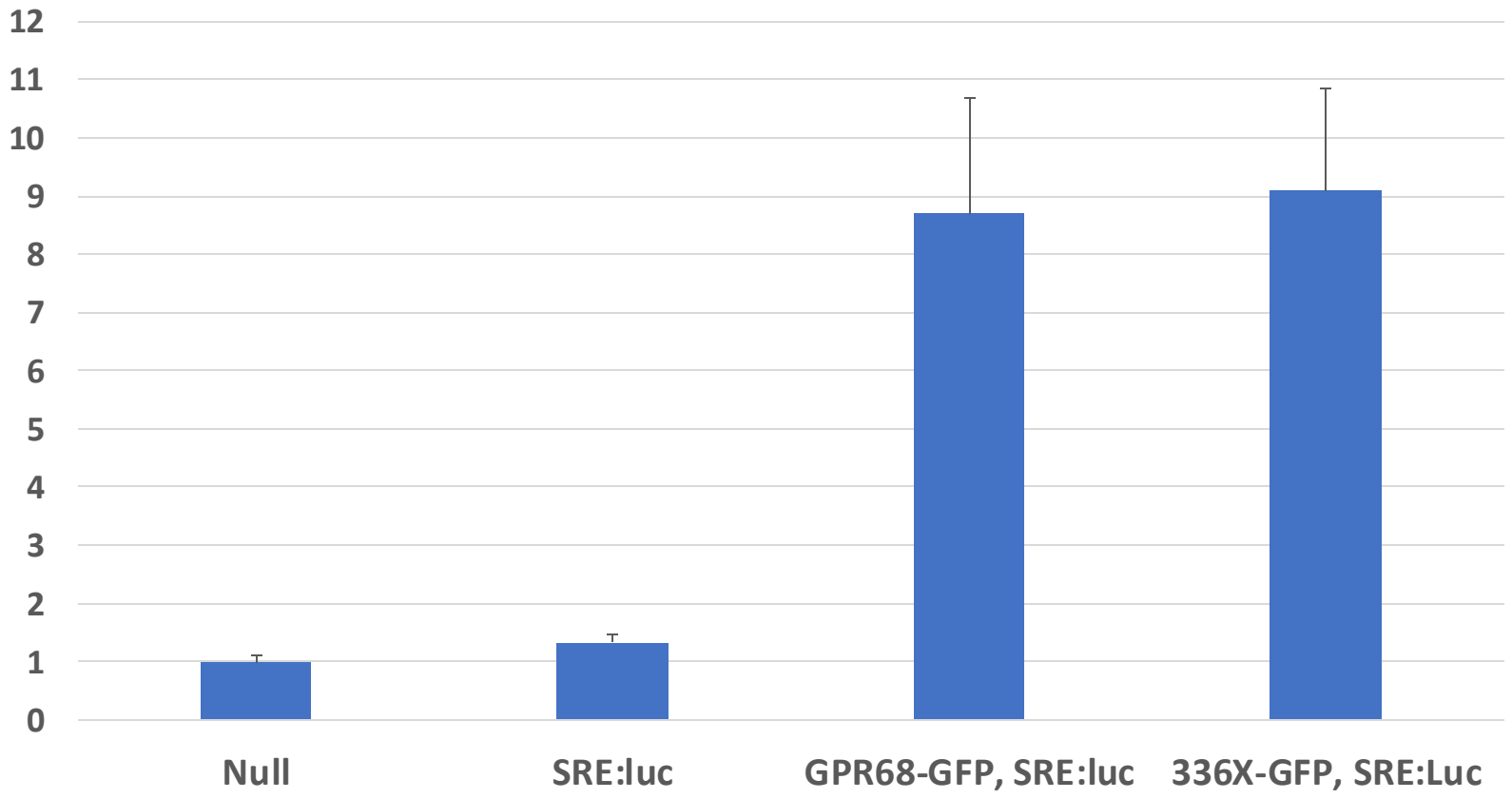
12
11
10
9
8
7
6
5
4
3
2
1
0
Null
SRE:luc
GPR68-GFP, SRE:luc
336X-GFP, SRE:Luc

Sup 6

A

Molecule	Concentration	Target	Phenotype
DMSO	1%	Vehicle	Normal
Phlorizin	600uM	Na/glucose antagonist	Normal
Bafilomycin	1uM	V-atpase antagonist	Toxic
Concanamycin	1uM	V-atpase antagonist	Toxic
Omeprazole	60uM	H/K atpase antagonist	Phenocopy
Lansoprazole	600uM	H/K atpase antagonist	Phenocopy
EIPA	25uM	NHE antagonist	Developmental delay

B

Sup 7